OPEN

Giant electrical modulation of magnetization in $Co_{40}Fe_{40}B_{20}$/$Pb(Mg_{1/3}Nb_{2/3})_{0.7}Ti_{0.3}O_3(011)$ heterostructure

Sen Zhang[1,2], Yonggang Zhao[1,3], Xia Xiao[4], Yizheng Wu[4], Syed Rizwan[5], Lifeng Yang[1], Peisen Li[1], Jiawei Wang[1], Meihong Zhu[1], Huiyun Zhang[1], Xiaofeng Jin[4] & Xiufeng Han[5]

[1]Department of Physics and State Key Laboratory of Low-Dimensional Quantum Physics, Tsinghua University, Beijing 100084, P. R. China, [2]College of Science, National University of Defense Technology, Changsha 410073, P. R. China, [3]Collaborative Innovation Center of Quantum Matter, Beijing 100084, P. R. China, [4]Department of Physics, State Key Laboratory of Surface Physics and Advanced Materials Laboratory, Fudan University, Shanghai 200433, P. R. China, [5]Beijing National Laboratory for Condensed Matter Physics, Chinese Academy of Sciences, Beijing 100190, P. R. China.

Correspondence and requests for materials should be addressed to S.Z. (zhangsen@nudt. edu.cn) or Y.G.Z. (ygzhao@tsinghua. edu.cn)

We report a giant electric-field control of magnetization (M) as well as magnetic anisotropy in a $Co_{40}Fe_{40}B_{20}$(CoFeB)/$Pb(Mg_{1/3}Nb_{2/3})_{0.7}Ti_{0.3}O_3$(PMN-PT) structure at room temperature, in which a maximum relative magnetization change ($\Delta M/M$) up to 83% with a 90° rotation of the easy axis under electric fields were observed by different magnetic measurement systems with *in-situ* electric fields. The mechanism for this giant magnetoelectric (ME) coupling can be understood as the combination of the ultra-high value of anisotropic in-plane piezoelectric coefficients of (011)-cut PMN-PT due to ferroelectric polarization reorientation and the perfect soft ferromagnetism without magnetocrystalline anisotropy of CoFeB film. Besides the giant electric-field control of magnetization and magnetic anisotropy, this work has also demonstrated the feasibility of reversible and deterministic magnetization reversal controlled by pulsed electric fields with the assistance of a weak magnetic field, which is important for realizing strain-mediated magnetoelectric random access memories.

Recently, multiferroic materials or structures, which simultaneously show two or more ferroic properties[1,2] such as ferroelectricity and ferromagnetism/ferrimagnetism, have drawn much interest due to the magnetoelectric (ME) coupling between the magnetic and ferroelectric (FE) orders and their potential applications in novel multi-functional devices[3,4]. Particularly, electric-field control of magnetism, known as the converse ME effect[5,6], has been extensively studied in multiferroic materials or structures, since it permits to manipulate magnetism by electric fields instead of magnetic fields or large currents, and provides an important access via electric-writing magnetic-reading for the next generation energy efficient memories[7,8].

To realize electric-field control of magnetization in multiferroic materials or structures, there are mainly three optional approaches[9,10]. The first choice is using intrinsic ME coupling in single phase multiferroics. However, single phase multiferroics are rather rare at room temperature and the converse ME effects are also typically too small to be useful[2]. It has been demonstrated that electric-field control of magnetism can be achieved in CoFe/$BiFeO_3$ structure via exchange coupling[11,12], however, in-plane electric fields were applied, which intrinsically prohibits the high storage capacity for memories[8]. The second choice is using electric field effect to induce the spin-polarized charge accumulation/dissipation at the interface, which results in a change in the interfacial magnetization[13]. This remarkable charge-mediated ME effect was observed at low temperatures, which is disadvantageous for applications. The third choice is strain-mediated ME effect in the heterostructures composed of ferromagnetic (FM) and FE materials through the transfer of piezostrain of the FE layer to the FM layer. Due to the vast choice of FE and FM materials, electric-field control of magnetism has been widely achieved in FM/FE heterostructures at room temperature with remarkable converse ME effects[5,14–19].

Regarding the electric-field manipulation of magnetism in multiferroic materials or structures, several factors are essential to realize electric-field-controlled magnetic random access memory. First of all, large magnetic response to electric stimuli should be performed at room temperature and therefore the strain-mediated ME

effects achieved in FM/FE multiferroic heterostructures become promising candidates[8]. In the FM/FE multiferroic heterostructures, the reports related to macroscopic piezostrain-mediated electric field control of magnetization are many[5,14–19], while work related to electric field control of magnetic anisotropy involving ferroelectric polarization reorientation is still less, which may hinder people from further understanding the mechanism and improving the ME effect in this system[9]. Secondly, directly electric-field control of magnetism with small or no magnetic field is more desirable. In most of the reports[14–16], electric-field control of magnetism was routinely achieved by measuring the magnetization-magnetic field (M-H) curves of the sample under different electric fields to show the converse ME effect. In this measurement, large external magnetic field up to the saturate field was needed and therefore electric-field control of magnetism in terms of magnetization-electric field (M-E) curves with small or no magnetic fields are more favorable[17,18]. Thirdly, reversible and deterministic reversal of magnetization is needed in magnetic recording. However, electric-field controlled 180° reversal of magnetization in FM/FE heterostructures at room temperature is still limited[12,19]. Moreover, FM materials employed in the spin-dependent transport devices, with high spin polarization and large magnetoresistance effect, are more preferred for ME coupling. $Co_{40}Fe_{40}B_{20}$ possesses the highest spin polarization among the amorphous ferromagnetic Co-Fe-B alloys[20], and has been demonstrated to achieve a very large tunneling magnetoresistance (TMR) in magnetic tunnel junctions (MTJs)[21]. On the other hand, FE single crystals such as lead magnesium niobate - lead titanate $Pb(Mg_{1/3}Nb_{2/3})_{0.7}Ti_{0.3}O_3$ exhibits ultra-high piezoelectric behavior[22], and has been reported to have a strong in-plane anisotropic piezostrain with electric fields applied along the [011] crystalline direction in the (011)-cut case[23,24]. Therefore, the combination of CoFeB thin film and PMN-PT(011) single crystal is an ideal candidate for achieving large ME effects and exploring the electric-field induced in-plane anisotropic piezostrain modulating on the magnetism of FM without magnetocrystalline anisotropy, which is important for realizing strain-mediated magnetoelectric random access memory (SME-RAM)[8].

In this paper, we report a giant electrical modulation of magnetization in a CoFeB/PMN-PT FM/FE structure at room temperature, with a maximum relative change $\Delta M/M$ up to 83%, which is much larger than those in the previous reports[17,18]. Magnetic Optic Kerr Effect with a rotating field (Rot-MOKE) was employed to investigate the magnetic anisotropy tuned by electric fields. Large magnetic anisotropy evolution with a 90° rotation of the easy axis above 5 kV/cm was observed due to the electric-field-induced in-plane strain anisotropy with the involvement of ferroelectric polarization reorientation. Moreover, magnetization reversal by pulsed electric fields was realized with the assistance of ±5 Oe magnetic fields, which is useful for magnetic recording devices.

Results

The brief configuration of the CoFeB/PMN-PT heterostructure consists of a 20 nm amorphous CoFeB film and a 0.2 mm (011)-cut PMN-PT single crystal as shown in Fig. 1(a), and the detailed fabricating processes are described in the *Methods Section*. The sample edges (*x*, *y* and *z*) were cut along the pseudo-cubic [100], [01-1] and [011] lattice directions of PMN-PT as shown in Fig. 1(b). The spontaneous polarizations of PMN-PT with rhombohedral (R) phase are along the <111> directions, i.e. the body diagonals of the pseudo-cubic unit cell in the (001)-cut case[22]. While in the (011)-cut case, the spontaneous polarizations lies along the diagonals of the (011) and (01-1) plane as shown in Fig. 1(b). The transformation between (001)-cut case and (011)-cut case as well as the corresponding X-ray diffraction patterns can be found in *Supplementary Information* (Fig. S1). The purpose of choosing this (011)-cut PMN-PT wafer is that PMN-PT single-crystal has a strong in-plane anisotropic piezostrain when electric field is applied along the [011] crystalline direction. The top view of the (011)-cut PMN-PT with spontaneous polarizations projecting on the (011) plane is shown in Fig. 1(c). When PMN-PT wafer is poled along the [011] direction by a positive
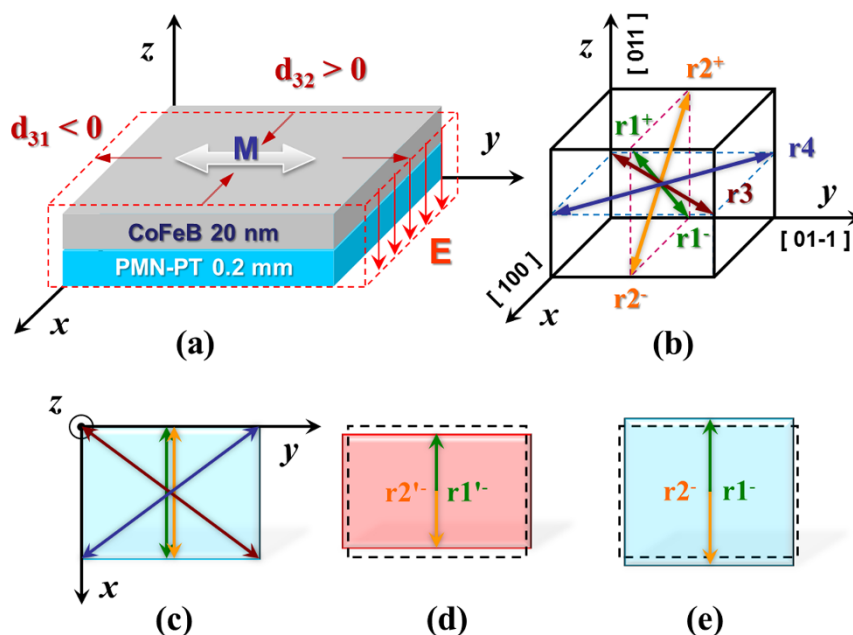

Figure 1 | Sketch of the sample, crystal structure and the polarizations of PMN-PT. (a) Configuration of the heterostructure, piezoresponse of the PMN-PT substrate and the easy axis of magnetization of the CoFeB layer under electric fields. (b) The unit cell and spontaneous polarizations of (011) oriented PMN-PT. (c), (d) and (e) Top view of the polarizations and deformation of the (011) crystal plane in PMN-PT substrate for the virgin state (c), under electric fields (d) and after removing electric fields (e). The slender arrows in (b), (c), (d) and (e) with the same color represent the same spontaneous polarizations of rhombohedral PMN-PT.

electric field, all of the eight possible polarization directions are switched downward with presence of only two of them, namely r1⁻ and r2⁻ as shown in Fig. 1. This means r3/r4 also change to r1⁻ and r2⁻. Larger electric fields rotate the polarizations r1⁻/r2⁻ toward the [0-1-1] direction (to be r1'⁻/r2'⁻), leading to a compressive strain along the [100] direction and an outstretched strain along the [01-1] direction as shown in Fig. 1(d). However, after removing the electric fields, all of the polarizations restore to r1⁻/r2⁻. As a result, the [100] direction is a little bit elongated as shown in Fig. 1(e) compared to the initial state as shown in Fig. 1(c), because the polarizations r3/r4 remain to be r1⁻/r2⁻. As reported in the literature[23,24], the (011)-cut PMN-30%PT we used here has the optimized orientation and composition to achieve ultra-high in-plane piezoelectric coefficients with $d_{31} \sim -3100$ pC/N along the [100] direction and $d_{32} \sim 1400$ pC/N along the [01-1] direction, respectively. This giant anisotropic piezostrain provides a great opportunity to generate a large in-plane magnetic anisotropic field and achieve a 90° rotation of the easy axis as well as a large magnetization response to electric field as shown in Fig. 1(a).

Electric-field control of magnetization was carried out in a Magnetic Property Measurement System (MPMS) with *in situ* electric fields and the detailed configuration can be found in our previous report[25]. Routinely, the magnetic hysteresis loops were firstly measured along the [100] direction and the [01-1] direction with electric fields of 0 kV/cm, 10 kV/cm and 20 kV/cm, respectively. The magnetization process of the sample along the [100] direction becomes harder and the remnant magnetization reduces when the electric field increases as shown in Fig. 2(a). However, the situation along the [01-1] direction is just the converse, with an increment of the M-H squareness under large electric fields as shown in the inset of Fig. 2(b). These results can be understood by the anisotropic strain of the (011)-cut PMN-PT under electric fields as discussed above, which generates an in-plane magnetic anisotropic field in CoFeB film. Since variable and large magnetic fields are not favorable for applications, investigation of directly electric-field control of magnetization with a fixed low magnetic field (H = 5 Oe) was performed, and the variations of magnetization with electric field along the two directions are shown in Figs. 2(c) and 2(d), respectively. The
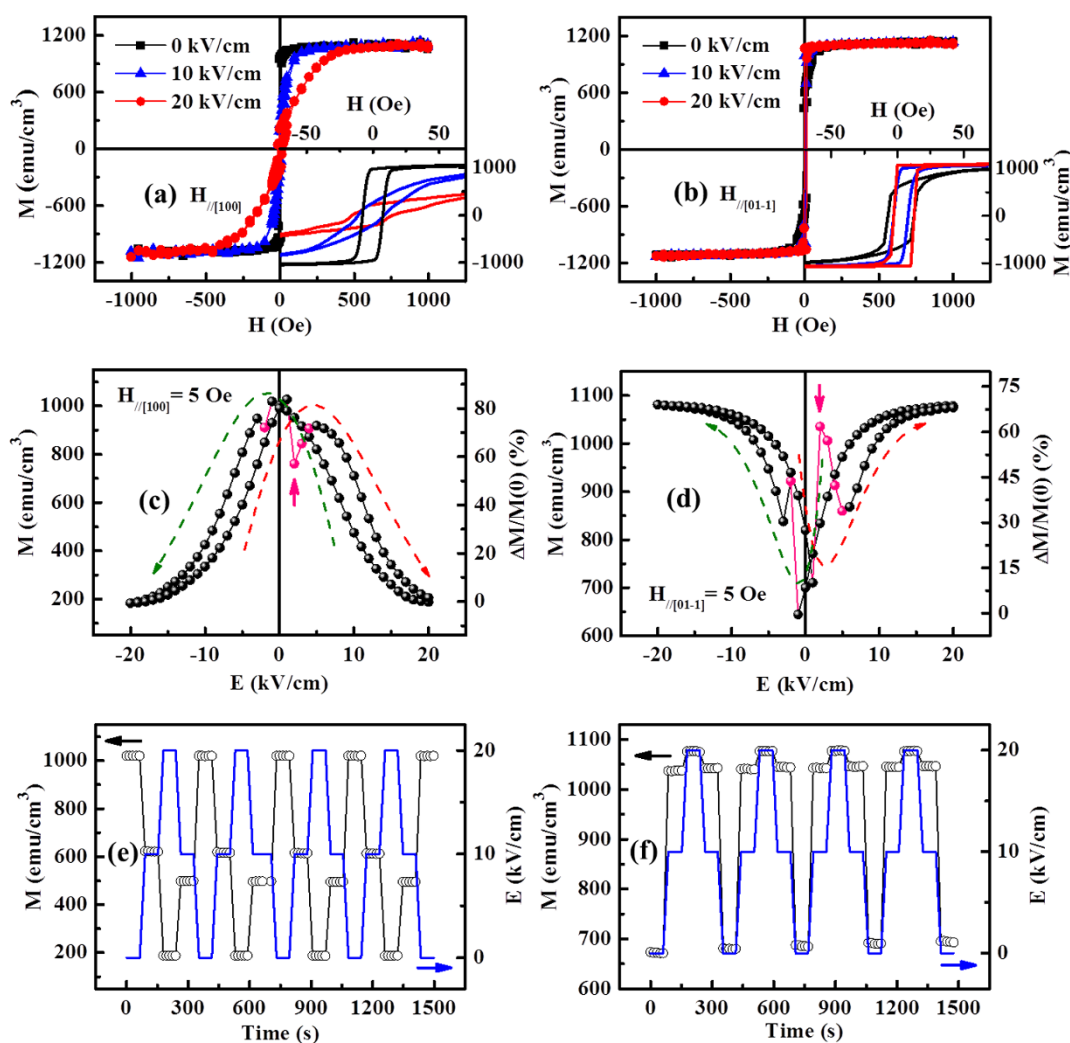

Figure 2 | Electric-field control of magnetization along the [100] and [01-1] directions. (a) Magnetic hysteresis loops measured along the [100] direction at $E = 0$ kV/cm (black square), 10 kV/cm (blue triangle) and 20 kV/cm (red circle), respectively. (b) M-H curves along the [01-1] direction under different electric fields. Insets of (a) and (b) show the expanded region of M-H at low magnetic fields. (c) Electric-field control of magnetization (black sphere) measured along the [100] direction with H = 5 Oe and the corresponding relative magnetization change *ΔM/M(0)*, where *M(0)* represents the magnetization at electric field of 0 kV/cm. (d) M-E curve along the [01-1] direction. The dashed arrows in (c) and (d) are guide for the sequence of measurements, and the pink points denoted by pink arrows are the *anomalous* points that jump away from the *butterfly-like* M-E curves due to ferroelectric domain switching. (e) The repeatable high/middle/low triple magnetization states (open circle) switched by electric fields (blue line) with $H_{//[100]}$ = 5 Oe. (f) Manipulation of magnetization by electric fields along the [01-1] direction.

magnetization response to electric field along the [100] direction exhibits a symmetrical *butterfly-like* behavior, similar to that in the previous reports in other FM/FE heterostructure[17,18]. However, from the M-E curve as shown in Fig. 2(c), one can see that the magnetization changes from above 1000 emu/cm^3 to lower than 200 emu/cm^3 with electric field changing from 0 kV/cm to 20 kV/cm, and the relative magnetization change [$\Delta M/M(0)$] is up to 83%, which is much larger than the previous results, such as 25% reported in La$_{0.7}$Sr$_{0.3}$MnO$_3$/PMN-PT[17] and 6% reported in CoFe$_2$O$_4$/PMN-PT[18]. By further optimizing the sample and reducing the bias magnetic field during the measurement, even larger $\Delta M/M(0)$ of 90% can be achieved (see details in Figs. S2 and S3 of *Supplementary Information*). This giant electrical modulation of magnetization originates from the combination of the ultra-high value of anisotropic in-plane piezoelectric coefficients of (011)-cut PMN-PT[23,24] and the perfect soft ferromagnetism without magnetocrystalline anisotropy of CoFeB film[26]. The M-E curve along the [01-1] direction also has a *butterfly-like* shape but with an opposite behavior compared to the curve along the [100] direction [Fig. 2(c)], i.e. electric field increases the magnetization from about 700 emu/cm^3 to near 1100 emu/cm^3 with $\Delta M/M(0) \sim 66\%$ as shown in Fig. 2(d). Moreover, we can see that there are several data points jumping away from the regular *butterfly-like* M-E curves, as masked by pink color and denoted by pink arrows in Figs. 2(c) and 2(d). These *anomalous* points are due to ferroelectric domain switching during the polarization reversal process (see details in Figs. S4 and S5 of *Supplementary Information*) and can be eliminated in the unipolar case (see details in Fig. S6 of *Supplementary Information*). Considering the requirements of applications, the stability and repeatability of the converse ME effect have

also been investigated. The sample was loaded by step-changed electric fields of 0 kV/cm, 10 kV/cm and 20 kV/cm in sequence with H = 5 Oe, and stable, repeatable and remarkable high/middle/low triple magnetization states were realized as shown in Figs. 2(e) and 2(f) for the [100] and [01-1] directions, respectively. As expected, the behavior along the [01-1] direction is reverse to that of the [100] direction, and the high/low magnetization ratios in them are about 1000 : 200 and 1100 : 700, which agree with M-E curves in magnitude as shown in Figs. 2(c) and 2(d) respectively. This should be very useful for the promising SME-RAMs[8].

In order to understand the electric-field control of magnetism and the origin of the giant electrical modulation of magnetization in our CoFeB/PMN-PT structure, Rot-MOKE method[27] with *in-situ* electric fields was employed to investigate the magnetic anisotropy tuned by electric fields. The basic configuration of the experiment is shown in Fig. 3(a) and the detailed process is described in the *Supplementary Information* (Fig. S7). Since the amorphous CoFeB has neither magnetocrystalline anisotropy nor induced magnetic anisotropy by external magnetic field during the fabrication, the initial state of the sample shows an in-plane magnetic isotropy[25]. When a large electric field ($E = 17.5$ kV/cm) was applied, a strong uniaxial magnetic anisotropy emerged with the easy axis along the [01-1] direction and a fitted uniaxial magnetic anisotropy field $H_u = 125$ Oe as revealed by the red torque curve in Fig. 3(b). However, after removing the electric field, a relative weak uniaxial magnetic anisotropy appeared with the easy axis turning to the [100] direction and a fitted uniaxial magnetic anisotropy field $H_u = 53$ Oe as revealed by the black torque curve in Fig. 3(b). The emergence of a strong uniaxial magnetic anisotropy with the easy axis along the [01-1]
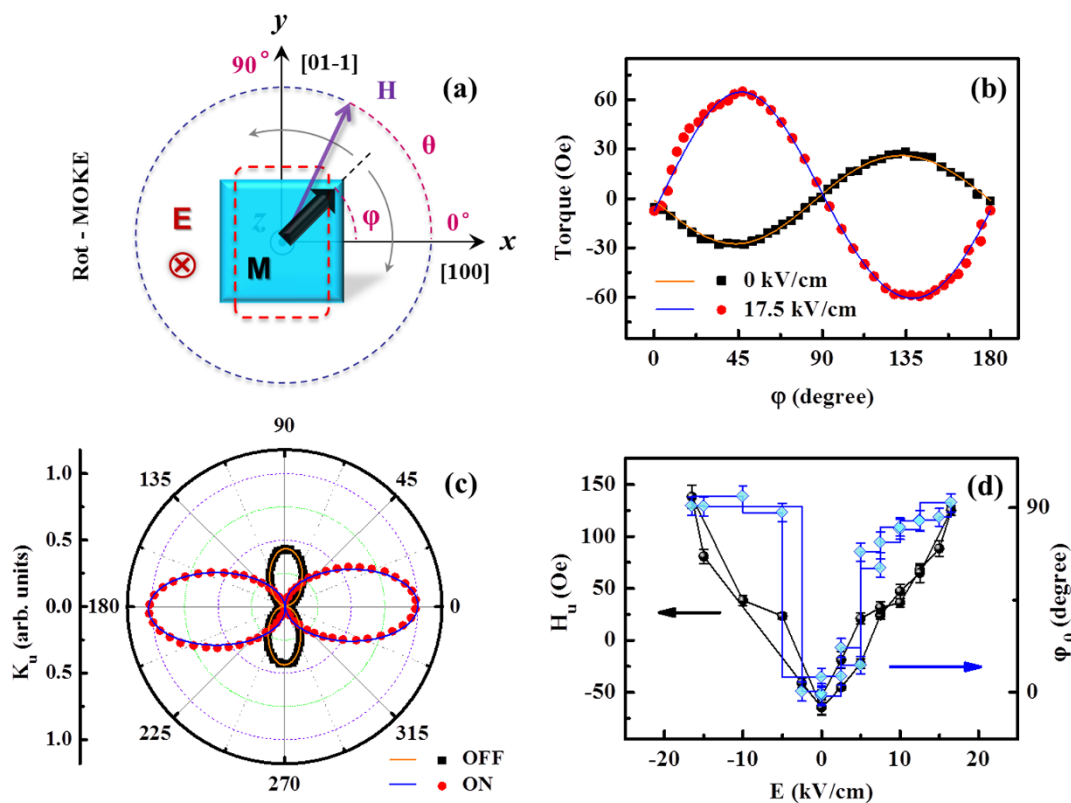

Figure 3 | Electric-field control of magnetic anisotropy characterized by Rot-MOKE method. (a) Configuration of the Rot-MOKE measurement and the definition of rotation angles (φ is the angle between the magnetization and the easy axis, θ is the angle between the external magnetic field and the easy axis). Dashed rectangle in (a) indicates the deformation of the sample under an electric field. (b) Calculated magnetic torque moment with E = 17.5 kV/cm (red circle) and E = 0 (black square) as a function of angle φ. (c) Polar graph of uniaxial anisotropy energy with $E = 17.5$ kV/cm on (red circle) and off (black square). (d) Amplitude of uniaxial magnetic anisotropy field (black sphere) and direction of the easy axis (blue rhombus) change with electric field, where φ_0 is the angle between the easy axis and the [100] direction. The colored curves in (b) and (c) are the theoretical results fitted from the experimental data, and error bars in (d) also come from the fitted values.

direction at large electric fields can be attributed to the appearance of the giant in-plane anisotropic strain under electric fields [Fig. 1(d)] and the positive magnetostriction coefficient ($\lambda_S \sim 3 \times 10^{-5}$) of the CoFeB film[26], while the emergence of weak uniaxial magnetic anisotropy after removal of electric field is unusual since the initial magnetic state of the sample showed an in-plane isotropy, and it can be understood as follows. As CoFeB was deposited on top of unpoled PMN-PT wafer, it shows an in-plane magnetic isotropy due to its amorphous nature and the randomness of ferroelectric domains in PMN-PT as shown in Fig. 1(c). After poling and removal of the electric field, all of the eight possible polarizations degenerate into r1⁻/r2⁻ as shown in Fig. 1(e). The transformation of r3/r4 to r1⁻/r2⁻ results in a compressive strain along the [01-1] direction and a tensile strain along the [100] direction, respectively. This anisotropic strain after poling induces a uniaxial magnetic anisotropy with easy axis along the [100] direction, increases the remnant magnetization along the [100] direction (compare the M-H curves at first 0 kV/cm and 2nd 0 kV/cm in Fig. S2(b) of *Supplementary Information*) and makes the value of magnetization at zero electric field along the [100] direction larger than that along the [01-1] direction [compare the values at zero electric field in Figs. 2(c) and 2(d)]. According to theory[27], the integration of magnetic torque moment $l(\varphi)$ over angle φ (the angle between magnetization and easy axis) gives the ratio between uniaxial anisotropy energy and saturation magnetization (K_u/M_S). Thus, the angle dependence of uniaxial anisotropy energy with electric field of 17.5 kV/cm on and off can be deduced as shown in Fig. 3(c), and one can distinctly see a 90°

rotation of the easy axis of the sample tuned by electric fields. To obtain the threshold electric field for rotation of the easy axis and the change of the induced uniaxial magnetic anisotropy field with electric field, magnetic torque measurement was carried out under a series of electric fields and different torque curves were obtained (see details in Fig. S7(d) of *Supplementary Information*). Fitting all the torque curves under different electric fields, magnetic anisotropy variation of the sample with electric field was obtained, and the fitted values of uniaxial magnetic anisotropy field (H_u) as well as the deduced orientations of easy axis (φ_0) are shown in Fig. 3(d). It reveals that the value of uniaxial magnetic anisotropy changes almost linearly from -53 Oe at zero electric field to about 130 Oe at $E = \pm 17.5$ kV/cm, and the direction of the easy axis stays along the [100] direction for electric fields below 5 kV/cm. However, the easy axis switches about 90° and lies along the [01-1] direction for electric fields above 5 kV/cm. The situation of the negative branch is almost the same, with a sharper easy axis switching process. Since the diameter of the light spot in the MOKE measurement is only 0.2 mm, we can also use it to investigate the electrical modulation of magnetization, which reveals the information of a local region near the sample surface instead of the bulk. These surface and local results as revealed by MOKE measurement (Figure S8 of *Supplementary Information*) are similar to those of bulk as revealed by MPMS measurement (Figure 2).

Utilizing this giant electrical modulation of magnetization, especially the electric-field controlled 90° rotation of the magnetic easy axis, a method of reversible and deterministic magnetization reversal
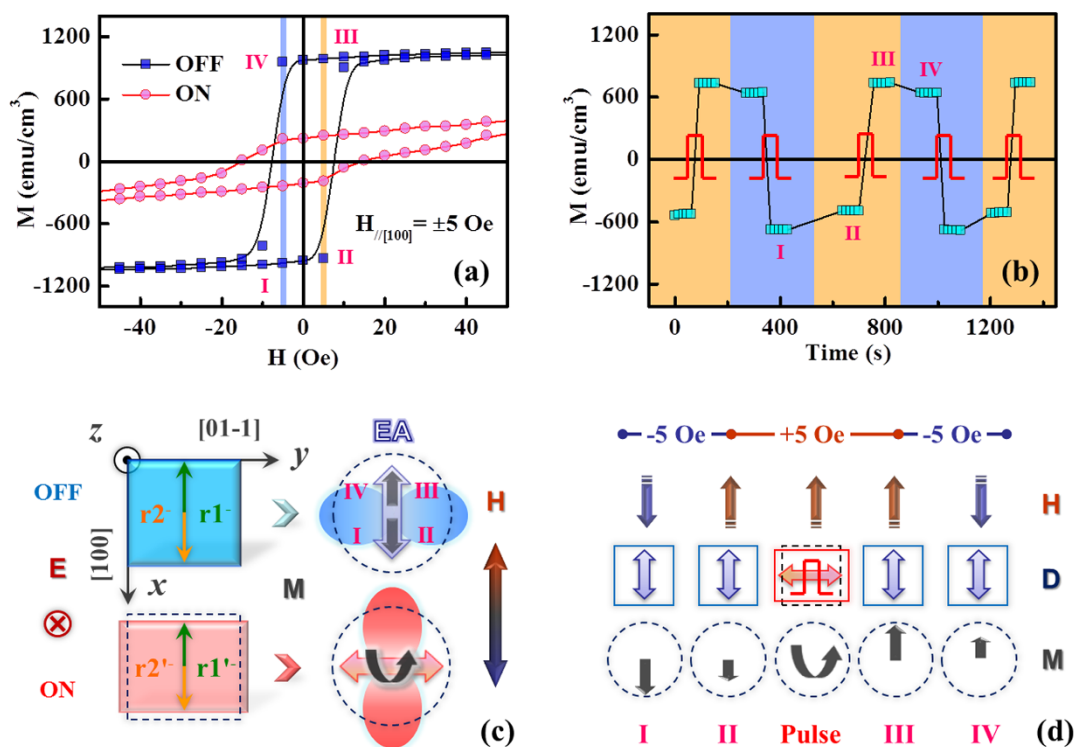

Figure 4 | Process of magnetization reversal controlled by pulsed electric fields with the assistance of magnetic fields H$_{//[100]}$ = ±5 Oe. (a) M-H curves with $E = 20$ kV/cm on (pink circle) and off (blue square) along the [100] direction. (b) Variation of magnetization (light blue square) with magnetic field and electric pulse (red line) at different time. (c) Configuration of the magnetization reversal by pulsed electric fields with the assistance of external magnetic fields (H). The left panel shows the deformation as well as polarizations in the (011) plane of PMN-PT controlled by switching electric field off/on and the right panel shows the induced magnetic anisotropy (denoted by colored dumbbells), easy axis (EA, denoted by broad bidirectional arrows) as well as magnetization (M, denoted by broad unidirectional arrows inside dashed circles and the broad bent arrow represents the magnetization which is rotating) change in the CoFeB film. (d) The sketch of the detailed switching process of magnetization controlled by pulsed electric fields, in which the auxiliary magnetic fields (H) are denoted by arrows with broken tails and the deformation (D) of the (011) crystal plane is denoted by a rectangle. The four different steps of magnetization denoted by letters I ∼ IV in (a) and (b) correspond to the diagrammatic states in (c) and (d), and the colors of the vertical bars in (a), background in (b) and arrows in (c) and (d) representing different magnetic fields are consistent.

controlled by pulsed electric fields and assisted with a weak magnetic field was demonstrated. One period of the manipulation is shown in Fig. 4. Firstly, the CoFeB film was magnetized by a large negative magnetic field and then the magnetization was measured at −5 Oe without electric field as denoted by stage I in Figs. 4(a) and 4(b). According to the previous discussions, the PMN-PT wafer is in a polarization state with $r1^-/r2^-$ dominant when the electric field is off, and the induced easy axis of magnetization is along the [100] direction as shown in the upper part of Fig. 4(c). In this situation, the magnetization is stable since magnetization, easy axis and external magnetic field are along the same direction (i.e. [100] direction) as shown in stage I of Fig. 4(d). Then, the magnetic field was switched to +5 Oe as denoted by stage II in Figs. 4(a) and 4(b). Since the coercive field of CoFeB is a little bit larger than 5 Oe, the +5 Oe magnetic field is not strong enough to switch the negative magnetization to the positive direction, and it only exhibits a minor change as shown in stage II of Fig. 4(b). However, this configuration is metastable because magnetization is antiparallel to the external magnetic field as shown in stage II of Fig. 4(d). Afterwards, a 20 kV/cm electric field was applied on the sample, resulting in a large in-plane anisotropic strain and rotation of the easy axis of magnetization to the [01-1] direction as shown in the lower part of Fig. 4(c). This sudden change of easy axis broke the metastable state in stage II and the negatively aligned magnetization began to rotate towards the positive direction as shown in Fig. 4(d). Afterwards, the electric field was turn off and the PMN-PT wafer changed back to $r1^-/r2^-$ dominant state, which rotated the easy axis of magnetization back to the [100] direction as shown in the upper part of Fig. 4(c), leading to another stable state with magnetization, easy axis and external magnetic field along the same direction as shown in stage III of Fig. 4(d) and a large positive magnetization state as shown in stage III of Figs. 4(a) and 4(b). Similar processes were taken by switching the magnetic field to −5 Oe [stage IV in Figs. 4(a), 4(b) and 4(d)], followed by another pulsed electric field, and similar behavior was observed as the previous case with magnetization switched to the negative direction as shown in Fig. 4(b). This magnetization reversal process, controlled by pulsed electric fields and assisted with a weak magnetic field, is repeatable, holding promise for applications in the novel multifunctional devices.

Discussion

Regarding the electric-field-controlled magnetization reversal, the magnetoelectric Cr_2O_3 has also played an important role in the vertical exchange coupling system. Via magnetoelectric field cooling, magnetoelectric switching of exchange bias can be achieved in a magnetoelectric $Cr_2O_3(111)/(Co/Pt)_3$ heterostructure[28], which has been proposed and designed as voltage controlled spintronic devices assisted with local heating[29]. Under sufficient large field product **E·H**, isothermal electric control of exchange bias can also be achieved at room temperature[30], with promising applications. Compared with the vertical exchange coupling Cr_2O_3 system with magnetization switched up/down, the strain-mediated electrical modulation of magnetization as reported here is operated with magnetization rotated in plane, which is highly relevant to the proposed SME-RAMs[8] and helpful for further realizing electric-writing magnetic-reading spintronic devices related to CoFeB[21]. Besides, the operation electric field in the CoFeB/PMN-PT structure is relatively low and can be further reduced by optimizing the strain transfer efficiencies (see details in Fig. S9 of *Supplementary Information*), which is important for energy efficient magnetic-electric devices.

In summary, giant electrical modulation of magnetization at room temperature is reported in a heterostructure composed of amorphous ferromagnetic $Co_{40}Fe_{40}B_{20}$ and (011)-cut $Pb(Mg_{1/3}Nb_{2/3})_{0.7}Ti_{0.3}O_3$ with a maximum relative magnetization change up to 83%. Rot-MOKE measurement demonstrated a 90° rotation of the easy axis above 5 kV/cm due to the electric field induced in-plane strain anisotropy related to ferroelectric polarization reorientation, which leads to the giant modulation of magnetization. With the assistance of a weak magnetic field, reversible and deterministic magnetization reversal controlled by pulsed electric fields has been achieved, holding promising applications for the novel multifunctional devices.

Methods

1. Spaldin, N. A. & Fiebig, M. The renaissance of magnetoelectric multiferroics. *Science* **309**, 391–392 (2005).
2. Eerenstein, W., Mathur, N. D. & Scott, J. F. Multiferroic and magnetoelectric materials. *Nature* **442**, 759–765 (2006).
3. Fiebig, M. Revival of the magnetoelectric effect. *J. Phys. D: Appl. Phys.* **38**, R123–R152 (2005).
4. Spaldin, N. A., Cheong, S. W. & Ramesh, R. Multiferroics: Past, present, and future. *Phys. Today* **63**, 38–43 (2010).
5. Eerenstein, W., Wiora, M., Prieto, J. L., Scott, J. F. & Mathur, N. D. Giant sharp and persistent converse magnetoelectric effects in multiferroic epitaxial heterostructures. *Nat. Mater.* **6**, 348–351 (2007).
6. Tokura, Y. Multiferroics-toward strong coupling between magnetization and polarization in a solid. *J. Magn. Magn. Mater.* **310**, 1145–1150 (2007).
7. Bibes, M. & Barthelemy, A. Multiferroics: Towards a magnetoelectric memory. *Nat. Mater.* **7**, 425–426 (2008).
8. Hu, J. M., Li, Z., Chen, L. & Nan, C. High-density magnetoresistive random access memory operating at ultralow voltage at room temperature. *Nat. Commun.* **2**, 533 (2011).
9. Ma, J., Hu, J. M., Li, Z. & Nan, C. W. Recent progress in multiferroic magnetoelectric composites: from bulk to thin films. *Adv. Mater.* **23**, 1062–1087 (2011).
10. Vaz, C. A. F. Electric field control of magnetism in multiferroic heterostructures. *J. Phys.: Condens. Matter.* **24**, 333201 (2012).
11. Chu, Y. H. *et al.* Electric-field control of local ferromagnetism using a magnetoelectric multiferroic. *Nat. Mater.* **7**, 478–482 (2008).
12. Heron, J. T. *et al.* Electric-field-induced magnetization reversal in a ferromagnet-multiferroic heterostructure. *Phys. Rev. Lett.* **107**, 217202 (2011).
13. Molegraaf, H. J. A. *et al.* Magnetoelectric effects in complex oxides with competing ground states. *Adv. Mater.* **21**, 3470–3474 (2009).
14. Lou, J., Liu, M., Reed, D., Ren, Y. H. & Sun, N. X. Giant electric field tuning of magnetism in novel multiferroic FeGaB/lead zinc niobate-lead titanate (PZN-PT) heterostructures. *Adv. Mater.* **21**, 4711–4715 (2009).
15. Liu, M. *et al.* Giant electric field tuning of magnetic properties in multiferroic ferrite/ferroelectric heterostructures. *Adv. Funct. Mater.* **19**, 1826–1831 (2009).
16. Wu, T. *et al.* Giant electric-field-induced reversible and permanent magnetization reorientation. *Appl. Phys. Lett.* **98**, 012504 (2011).
17. Thiele, C., Dorr, K., Bilani, O., Rodel, J. & Schultz, L. Influence of strain on the magnetization and magnetoelectric effect in $La_{0.7}A_{0.3}MnO_3$/PMN-PT(001) (A = Sr,Ca). *Phys. Rev. B* **75**, 054408 (2007).
18. Yang, J. J. *et al.* Electric field manipulation of magnetization at room temperature in multiferroic heterostructures. *Appl. Phys. Lett.* **94**, 212504 (2009).
19. Chen, Y. J., Fitchorov, T., Vittoria, C. & Harris, V. G. Electrically controlled magnetization switching in a multiferroic heterostructure. *Appl. Phys. Lett.* **97**, 052502 (2010).
20. Kubota, T., Daibou, T., Oogane, M., Ando, Y. & Miyazaki, T. Tunneling spin polarization and magnetic properties of Co-Fe-B alloys and their dependence on boron content. *Jpn. J. Appl. Phys.* **46**, L250–L252 (2007).
21. Ikeda, S. *et al.* Tunnel magnetoresistance of 604% at 300 K by suppression of Ta diffusion in CoFeB/MgO/CoFeB pseudo-spin-valves annealed at high temperature. *Appl. Phys. Lett.* **93**, 082508 (2008).
22. Park, S. E. & Shrout, T. R. Ultrahigh strain and piezoelectric behavior in relaxor based ferroelectric single crystals. *J. Appl. Phys.* **82**, 1804–1811 (1997).
23. Peng, J. *et al.* Orientation dependence of transverse piezoelectric properties of $0.70Pb(Mg_{1/3}Nb_{2/3})O_3$-$0.30PbTiO_3$ single crystals. *Appl. Phys. Lett.* **85**, 6221–6223 (2004).
24. Luo, L. *et al.* Ultrahigh transverse strain and piezoelectric behavior in $(1-x)Pb(Mg_{1/3}Nb_{2/3})O_3$-$xPbTiO_3$ crystals. *J. Appl. Phys.* **99**, 24104 (2006).

25. Zhang, S. *et al.* Electric-field control of nonvolatile magnetization in $Co_{40}Fe_{40}B_{20}$/$Pb(Mg_{1/3}Nb_{2/3})_{0.7}Ti_{0.3}O_3$ structure at room temperature. *Phys. Rev. Lett.* **108**, 137203 (2012).
26. Jen, S. U. *et al.* Magnetic and electrical properties of amorphous CoFeB films. *J. Appl. Phys.* **99**, 053701 (2006).
27. Mattheis, R. & Quednau, G. Determination of the anisotropy field strength in ultra-thin magnetic films using longitudinal MOKE and a rotating field: the ROTMOKE method. *J. Magn. Magn. Mater.* **205**, 143–150 (1999).
28. Borisov, P., Hochstrat, A., Chen, X., Kleemann, W. & Binek, C. Magnetoelectric switching of exchange bias. *Phys. Rev. Lett.* **94**, 117203 (2005).
29. Chen, X., Hochstrat, A., Borisov, P. & Kleemanna, W. Magnetoelectric exchange bias systems in spintronics. *Appl. Phys. Lett.* **89**, 202508 (2006).
30. He, X. *et al.* Robust isothermal electric control of exchange bias at room temperature. *Nat. Mater.* **9**, 579–585 (2010).

Acknowledgments

Author contributions

S.Z. designed the multiferroic structure and performed the experiments. Y.G.Z. directed the research. X.X. and Y.Z.W. carried out the MOKE measurements and analyzed the MOKE data. S.R. grew the CoFeB film. L.F.Y., P.S.L. and J.W.W. assisted in the measurements of magnetic property. S.Z. and Y.G.Z. prepared the manuscript and refined the paper. M.H.Z., H.Y.Z., X.F.J. and X.F.H. supervised the experiments and made scientific comment on the manuscript. All authors discussed the results and contributed to the refinement of the paper.

Additional information

How to cite this article: Zhang, S. *et al.* Giant electrical modulation of magnetization in $Co_{40}Fe_{40}B_{20}$/$Pb(Mg_{1/3}Nb_{2/3})_{0.7}Ti_{0.3}O_3(011)$ heterostructure. *Sci. Rep.* **4**, 3727; DOI:10.1038/srep03727 (2014).